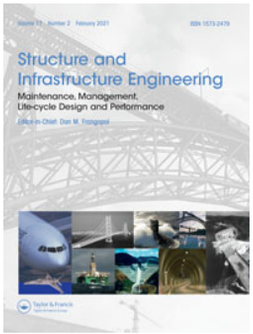

Taylor & Francis
Taylor & Francis Group

Structure and Infrastructure Engineering
Maintenance, Management, Life-Cycle Design and Performance

ISSN: 1573-2479 (Print) 1744-8980 (Online) Journal homepage: https://www.tandfonline.com/loi/nsie20

Numerical investigation on progressive collapse resistance of steel-concrete composite floor systems

Junjie Wang, Wei Wang, Yihai Bao & Dawn Lehman

To cite this article: Junjie Wang, Wei Wang, Yihai Bao & Dawn Lehman (2021) Numerical investigation on progressive collapse resistance of steel-concrete composite floor systems, Structure and Infrastructure Engineering, 17:2, 202-216, DOI: 10.1080/15732479.2020.1733622

To link to this article: https://doi.org/10.1080/15732479.2020.1733622

STRUCTURE AND INFRASTRUCTURE ENGINEERING
2021, VOL. 17, NO. 2, 202–216
https://doi.org/10.1080/15732479.2020.1733622

Numerical investigation on progressive collapse resistance of steel-concrete composite floor systems

Junjie Wang[a,b,c], Wei Wang[a,b], Yihai Bao[d] and Dawn Lehman[c]

[a]State Key Laboratory of Disaster Reduction in Civil Engineering, Tongji University, Shanghai, China; [b]Department of Structural Engineering, Tongji University, Shanghai, China; [c]Civil & Environmental Engineering, University of Washington, Seattle, WA, USA; [d]Independent Consultant Engineer, Gaithersburg, MD, USA

ABSTRACT

Steel-concrete composite floor systems are commonly used in steel buildings. Stability under gravity and lateral loading depends on these systems. To better understand the design parameters that govern the progressive collapse behaviour of steel-concrete composite floor systems, high-resolution finite-element analyses (FEA) is conducted. Steel fracture and concrete damage are explicitly considered in the finite-element model (FEM). The model is validated using full-scale test data including comparison of the measured response and failure modes. The validated model is used to conduct a parametric study to investigate untested parameters including (i) concrete strength, (ii) horizontal constraint, (iii) steel deck thickness, (iv) reinforcement ratio in the composite slab, and (v) the number of the shear studs. The simulation results are used to determine the optimum design to increase progressive collapse resistance. Specifically, it is found that increasing the continuity and the horizontal constraint of the steel deck, the steel deck thickness, and number of shear studs increase this resistance. Considering the steel consumption and the common practice in the construction, improving the continuity and the horizontal constraint of the steel deck are the best choices to improve the collapse resistance.

ARTICLE HISTORY
Received 25 August 2019
Revised 9 November 2019
Accepted 27 December 2019

KEYWORDS
Composite slabs; disproportionate collapse; finite element method; floor systems; progressive collapse; membrane action

1. Introduction

The steel-concrete composite floor system, which is designed to resist gravity load, is widely adopted in the steel-framed buildings. The composite floor system is also a primary contributor to protect the structures from progressive collapse, which is supported by the numerical simulations conducted by Sadek, El-Tawil, and Lew (2008), Alashker, El-Tawil, and Sadek (2010), Alashker and El-Tawil (2011). In recent years, several three-dimensional large-scale steel-concrete composite floor systems have been experimentally tested under the column removal scenario (Fu, Tan, Zhou, & Yang, 2017, 2018; Hadjioannou, Donahue, Williamson, & Engelhardt, 2018; Johnson, Meissner, & Fahnestock, 2016; Wang, Wang, & Bao, 2020; Wang, Wang, Bao, & Lehman, 2019). To simulate the uniformly distributed load on the slab, the tests conducted by Johnson et al. (2016) and Hadjioannou et al. (2018) were loaded by pumping water into the tanks placed on the slab, while the other tests were loaded by the actuator through load-distribution beams. All the tests exhibited significant load-carrying capacities with the help of the composite slabs. If the lateral movements at the boundary of the tested specimens were constrained, the tensile membrane action was observed in the composite floor prior to the collapse.

The tensile membrane action in the reinforced concrete slab has been investigated since decades ago (Hayes, 1968; Park, 1964a, 1964b, 1965; Sawczuk & Winnicki, 1965). Considering the progressive collapse is a low probability event, the tensile membrane action can be seen as an economical secondary load-carrying mechanism to resist progressive collapse without significantly increase construction expenses. Hence, many researchers (Botte, Gouverneur, Caspeele, & Taerwe, 2015; Gouverneur, Caspeele, & Taerwe, 2013a, 2013b, 2015; Mitchell & Cook, 1984; Qian, Li, & Ma, 2015; Yi, Zhang, & Kunnath, 2014) theoretically or experimentally investigated the development of the tensile membrane action in the reinforced concrete slab under progressive collapse scenario. In the reinforced concrete slab, the tensile membrane action only comes from the slab reinforcement. However, for the composite floor, the steel deck may develop more membrane force than the slab reinforcement (Alashker et al., 2010). Nevertheless, up to now, there are limited researches focused on the steel deck's contribution to the tensile membrane action.

Except the collapse mode governed by the floor failure, the collapse mode may also be governed by the column buckling failure (Bao, Main, & Noh, 2017; Gerasimidis, 2014; Gerasimidis, Deodatis, Kontoroupi, & Ettouney, 2015; Gerasimidis, Deodatis, Yan, & Ettouney, 2017). Particularly, when the column removal location is at the low floors of the tall frame structures, the column buckling failure is more likely to be the dominant collapse mode. However,

CONTACT Wei Wang weiwang@tongji.edu.cn State Key Laboratory of Disaster Reduction in Civil Engineering, Tongji University, Shanghai, China

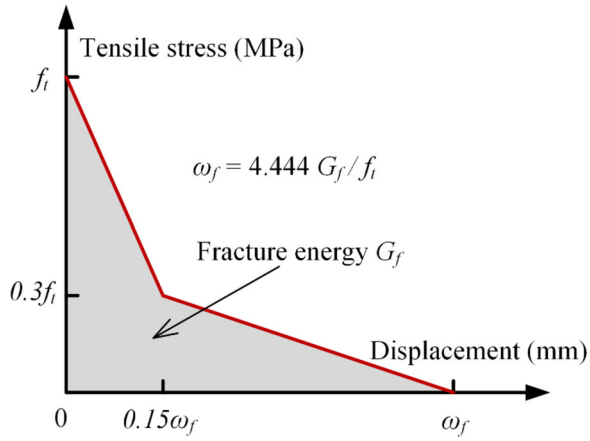

Figure 1. Uniaxial tensile softening relationship for concrete.

the column buckling failure can be avoided by enlarging the column cross-section to withstand the potential redistributed gravity load. Therefore, the column buckling failure is not taken into consideration in this paper.

In this paper, the development of the tensile membrane action in the composite floor is the primary research objective. High-resolution finite-element analyses (FEA) are used to conduct parametric studies on the influence of boundary constraint, steel deck continuity and thickness, slab reinforcement ratio and layout, concrete strength, and shear stud quantities. The reliability of the finite-element model (FEM) used in this paper has been validated by comparing it with a full-scale composite floor test (Wang et al., 2020). The influences of the stress triaxiality and Lode angle on the ductile fracture of the steel have been carefully modelled. Besides, the nonlinear behaviour and damage evolution of the concrete have also been considered. All the simulations in this paper are conducted in LS-DYNA R9.1 (Hallquist, 2016).

2. Modelling scheme

This section describes the element types and material models used in the analysis of the steel-concrete composite floor system under column removal scenario.

2.1. Element formulation and material model for steel

The girders, beams, columns, and steel decks are modelled with 4-node shell elements, which use the Belytschko-Lin-Tsay Shell formulation proposed by Belytschko, Lin, and Chen-Shyh (1984). Owing to its superior efficiency, the Belytschko-Lin-Tsay Shell is most commonly used in the explicit simulation. To expedite computational speed, the steel reinforcement is modelled with truss elements, which only carry the axial force. The shear studs are modelled using Hughes-Liu beam elements, which formulation is based on the Hughes-Liu shell (Hughes & Liu, 1981a, 1981b). The advantages of Hughes-Liu beam element are computational efficiency, robustness, and compatibility with solid elements.

The inelastic behaviour of the girders, beams, columns, steel decks, and shear studs are modelled by the piecewise-linear plasticity model (Material 24 in LS-DYNA). The welded steel reinforcement is using the bilinear elastic-plastic model proposed by Krieg and Key (1976). The nominal stress-nominal strain (σ_{nom}-ε_{nom}) curves are converted into the true stress-true strain (σ-ε) curves with Equations (1) and (2). The σ-ε curves are used to specify the material model parameters. Fracture of steels is simulated by removing the element from the model when the specified failure strain was reached. The determination procedures of the steel fracture strain are described in detail by Wang, Wang, and Qian (2019), which considers the influences of the stress triaxiality and Lode angle:

$$\sigma = \sigma_{\text{nom}}(1 + \varepsilon_{\text{nom}}) \tag{1}$$

$$\varepsilon = \ln(1 + \varepsilon_{\text{nom}}) \tag{2}$$

2.2. Element formulation and material model for concrete

The concrete slab is modelled with 8-node, reduced-integration solid elements (one integration point in each solid element), which can substantially reduce the computational time. The Flanagan-Belytschko stiffness form with exact volume integration for the solid element method (Hallquist, 2016) is used to prevent the zero-energy deformation mode (hourglass deformation mode).

The constitutive model used for the solid elements represented concrete slab is the concrete damage plasticity model, which is proposed by Grassl and Jirásek (2006), Grassl, Xenos, Nyström, Rempling, and Gylltoft (2013). This model is capable of describing the realistic nonlinear behaviour of the concrete, including stiffness degradation, irreversible displacements, confinement effect, and damage evolution. As illustrated in Figure 1, the bilinear softening response is selected to represent the concrete damage evolution under tension. In Figure 1, f_t is the maximum tensile strength of concrete, and ω_f is the nonlinear displacement when the tensile stress of concrete reduces to zero. The stress-displacement response can be converted into stress-strain response via $\varepsilon_t = \omega_f/l_e$, where ε_t is the plastic strain when the tensile stress reduces to zero, l_e is the characteristic length of the element. The softening response of concrete is affected by the fracture energy of concrete (G_f), which can be obtained by (CEB-FIP, 2010):

$$G_f = 73\ f_c^{0.18} \tag{3}$$

in which, f_c is the compressive strength of concrete.

2.3. Contact properties

The contacts between steel members and concrete slab, and the contacts between steel decks and other steel members are modelled using the automatic surface-to-surface contact algorithm with a friction coefficient of 0.5 (Tahmasebinia, Ranzi, & Zona, 2011). Tie constraints are selected to model the interaction between girders, beams, and columns. The welded steel reinforcement and the shear stud are perfectly bonded to the concrete slab, and the slips between these parts are neglected. The shear studs are constrained to the

beams or girders by spring elements, which properties are derived from the load-deformation responses of the push-out tests.

3. FEM validation

The modelling methodology described above is used to simulate a full-scale steel-concrete composite floor system test conducted by Wang et al. (2020). The test setup and specimen details are shown in Figure 2. This specimen, which represents the middle edge column removal scenario, is extracted from a five-story steel-concrete composite frame structure. The design dead load is 5 kN/m^{2,} and the live load is 2 kN/m^2. The design basic earthquake acceleration is 0.1 g, and the design basic wind pressure is 0.55 kN/m^2. The girder span, beam span, and story height are 4.2 m, 3.6 m, and 3.6 m, respectively. The structural layout of each floor is identical, and the first floor of the prototype structure is shown in Figure 3. The steel braces are designed to resist the lateral loads in the prototype structure. The tested specimen represents the shaded area in Figure 3.

The connection details and slab sections are illustrated in Figure 4. The welded flange-bolted web (WFBW) connection is selected for the girder-to-column connection, while the simple shear-tab connection is selected for the beam-to-column connection and beam-to-girder connection. The bolts used in these connections are 16 mm in nominal diameter. The composite slab section consists a 50 mm high concrete slab and a 50 mm high trapezoidal steel deck. The thickness of the steel deck was 1.2 mm. The grid of the welded steel reinforcement is 200 × 200 mm. The diameter of the steel reinforcement is 8 mm, while the clear cover of them is 15 mm. Shear studs (16 mm in diameter and 80 mm in height) are used to connect the beams and composite slab. The spacings of shear stud along girder direction and beam direction are 300 mm and 305 mm, respectively.

As shown in Figure 2(b), the slab is extended by 900 mm to simulate the continuous boundary conditions provided by the neighbouring bays. The trapezoidal steel deck is continuous without any overlapping in the direction parallel to the girder. The welded steel reinforcement has a lap splice of 600 mm above the B5 and B6 beams, which could guarantee the continuity of the reinforcement. During the test, the constraints provided by the neighbouring bays are simulated by constraining the movements of the extended girders (G5, G6, G7, G8) and extended beams (B6, B7, B8). In the FEM (Figure 5(a)), all the translational degrees of freedom at the ends of G7, G8, B6, B7, and B8 are constrained. The translational degrees of freedom along the girder axis at the ends of G5 and G6 are constrained by a spring element, while the translational degrees of freedom in other directions are fully constrained. The stiffness of the spring element is 10 kN/mm, which is experimentally determined during the test.

During the test, the specimen is quasi-statically applied with displacement-controlled loads at 24 points (Figure 2(a)), which in order to simulate the uniformly distributed load on the slab. While in the FEM (Figure 5(a)), the uniform load is directly applied to the concrete slab in the two-bay area. The mechanical properties of steel materials are listed in Table 1, while the σ-ε curves used in the FEM are shown in Figure 6. The concrete compressive strength is obtained using three 150 mm × 150mm × 150mm cubes on the day of the test, whose compressive strengths are 33.1 MPa, 32.4 MPa, and 32.9 MPa. Therefore, the mean value of 33 MPa is taken as the cubic compressive strength. As listed in Table 2, the cubic strength is converted into the cylindrical strength (26 MPa) based on the CEB-FIP (2010). Based on Equation (3), the tensile strength, fracture energy, and elastic modulus are calculated as 2.7 MPa, 0.131 N/mm, and 29664 MPa, respectively. Figure 7 illustrates the stress-strain curve used for the concrete in this paper.

As shown in Figure 8, the shear responses of the shear stud along girder direction and beam direction are obtained from the push-out tests. The bilinear force-displacement curves in Figure 7 are used to define the shear properties of the spring element between the shear stud and steel beam. The failure displacements of this spring element are defined as the shear force reduced to 90% of the corresponding peak load (Eurocode, 2004). When the failure displacement is reached, the spring element will be deleted from the FEM. A relatively large stiffness is specified for these springs in other directions to prevent the failures in other directions.

Figure 5(b) depicts the mesh details in the FEM. The mesh size of the girder-to-column connection, beam-to-column connection, and beam-to-girder connection are 10 mm, while the mesh size in all other regions is 25 mm. More detailed description of the modelling procedures is introduced in Wang, Wang, and Qian (2019). Figure 9(a) presents the comparison between the analytical observation and experimental result in terms of vertical resistance versus vertical displacement at the removed column (C0). The force measured by the built-in load cell in the actuator is taken as the vertical resistance of the test specimen. In the FEM, the computed resultant vertical force at the column bases is taken as the load carried by the floor system. As shown in Figure 9(a), the presented FEM is capable of simulating the salient characteristics of the load-displacement curves, including the ascending, the softening and the re-ascending stage. Moreover, the failure of the girder-to-column connection and the fracture of the steel deck around this connection are successfully captured by the FEM, as shown in Figure 9(b). The crack patterns are shown using the tensile damage variable. Typically, wider crack results in a relatively larger tensile damage parameter. As shown in Figure 9(b), the distribution and orientation of the concrete cracks match well with the experimental results. These demonstrate the validity of the numerical model. Therefore, this modelling approach is used to investigate the key parameters that dominated the collapse behaviour of the steel-concrete composite floor system.

4. Parametric studies on the composite floor substructures

The validated numerical model is employed to explore the salient design parameters affecting collapse. The factors investigated include the lateral restraint stiffness at the

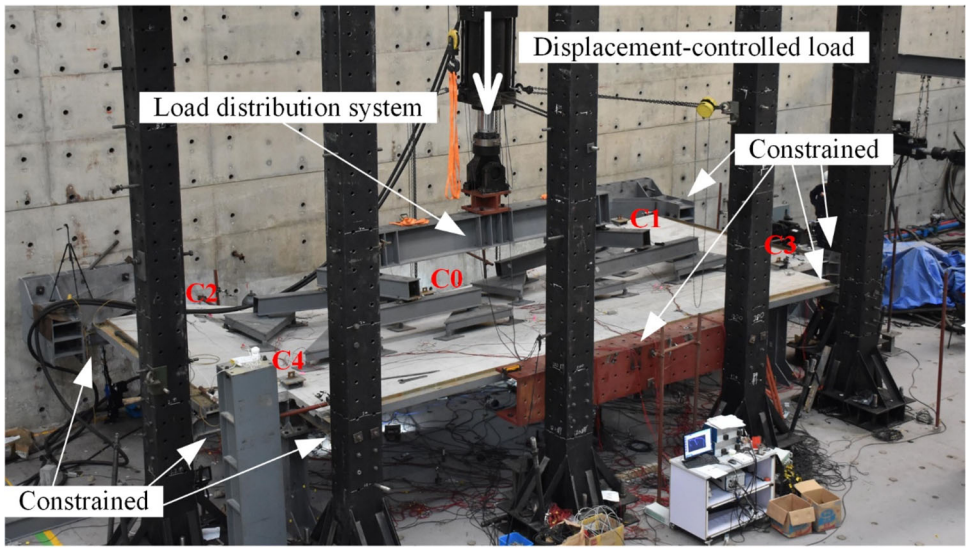

(a)

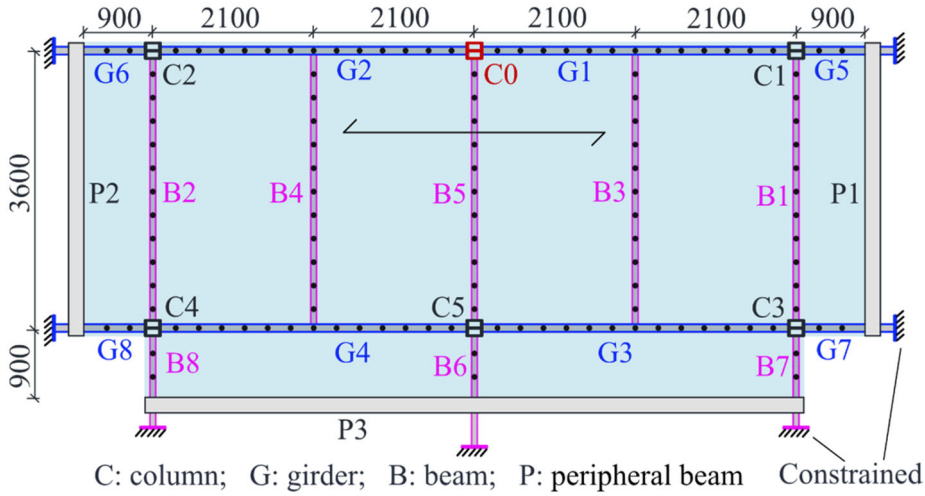

(b)

Figure 2. Test setup (a) and specimen dimensions (b) of the composite floor system.

horizontal boundaries, concrete strength, slab reinforcement ratio, slab reinforcement layout, steel deck thickness, the continuity of the steel deck, and the shear stud spacing.

4.1. Influence of concrete strength

Three simulations are conducted to investigate the influence of concrete strength as follows: (1) 26 MPa (identical to the experimental test), (2) 40 MPa, and (3) 60 MPa. The concrete properties are determined based on the CEB-FIP (2010), as listed in Table 2. The results of these three simulations are depicted in Figure 10. Comparing to the 26 MPa case, the vertical resistance is increased by 5% by increasing the concrete strength to 40 MPa. At the same time, the initial stiffness is also slightly improved at the flexural stage. Besides, the G1-C1 connection is fractured a little earlier with increasing the concrete strength from 26 MPa to 40 MPa. However, the load-displacement curves of the 40 MPa case and the 60 MPa case are almost identical. The results show that the concrete strength parameter is quite ineffectual, which is because the concrete could not provide much tensile force to improve the tensile membrane action. However, as noted by Fu (2010), even though increasing the tensile strength of the concrete has a limited contribution to the tying force, it could reduce the dynamic response of the structure under the column removal scenario.

4.2. Effect of the boundary condition

4.2.1. Boundary condition of girder

The influence of the boundary condition of girder is investigated by altering the horizontal constraint stiffness at the

ends of G5 and G6 girders. Three conditions are compared: (1) the horizontal movement is completely constrained, (2) the horizontal movement is completely released (i.e., not constrained) and (3) the horizontal constraint is partially constrained, which is identical to the experimental test.

The load-displacement curves of these three conditions are drawn in Figure 11. The maximum vertical force and corresponding vertical displacement are listed in Table 3.

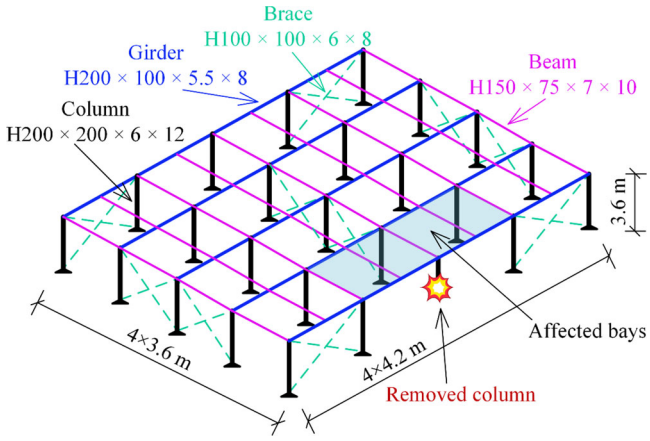

Figure 3. First floor of the prototype structure.

There is a continuously increasing trend of the load-displacement curve when the horizontal constraint is completely released. While the vertical load is increased, the exterior column C1 and C2 were also being pulled inward. If the lateral movement of the exterior column was too large, this column may be lost stability under the vertical force in the real structure (Bao et al., 2017). When the vertical displacement reaches 799 mm, the steel deck and welded steel reinforcement adjacent to the C1 and C2 columns are fractured, and the increasing trend of the load-displacement curve is also stopped. If the horizontal movement is completely constrained, the maximum vertical force is achieved at a much smaller displacement, 396 mm. At this moment, the G1-C1 connection and G2-C2 connection are completely failed. The vertical resistance could not be reinvigorated at a larger vertical displacement. If the horizontal movement is partially constrained, as the condition of the experimental test, the maximum vertical force is reached at a relatively larger deformation state. Furthermore, the vertical resistance in the partially constrained condition is the maximum value among all these three cases. As indicated by Table 3, increasing the stiffness of the horizontal boundary could decrease the vertical displacement of the maximum vertical force point, but might not increase the vertical resistance.

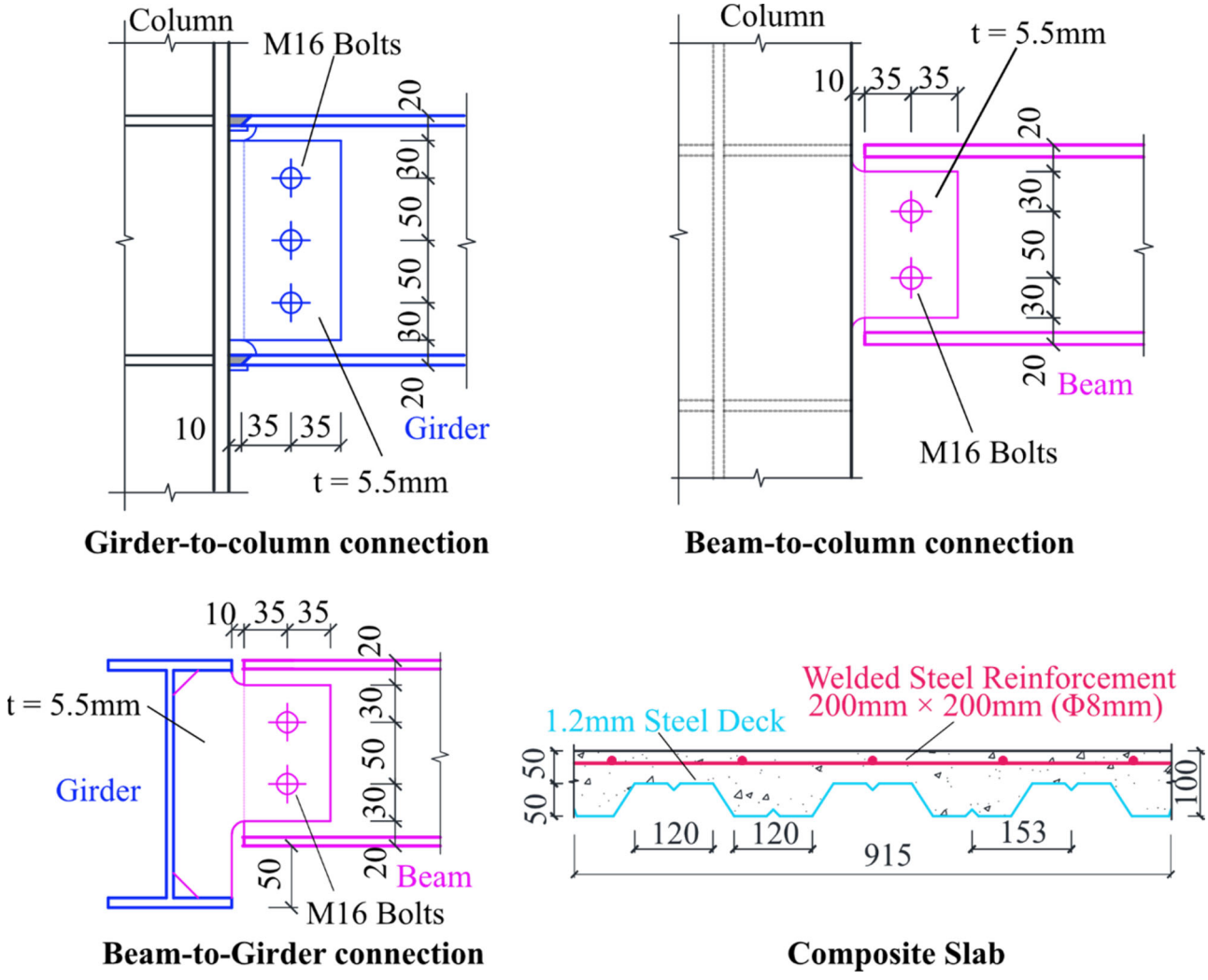

Figure 4. Connection details of the prototype structure.

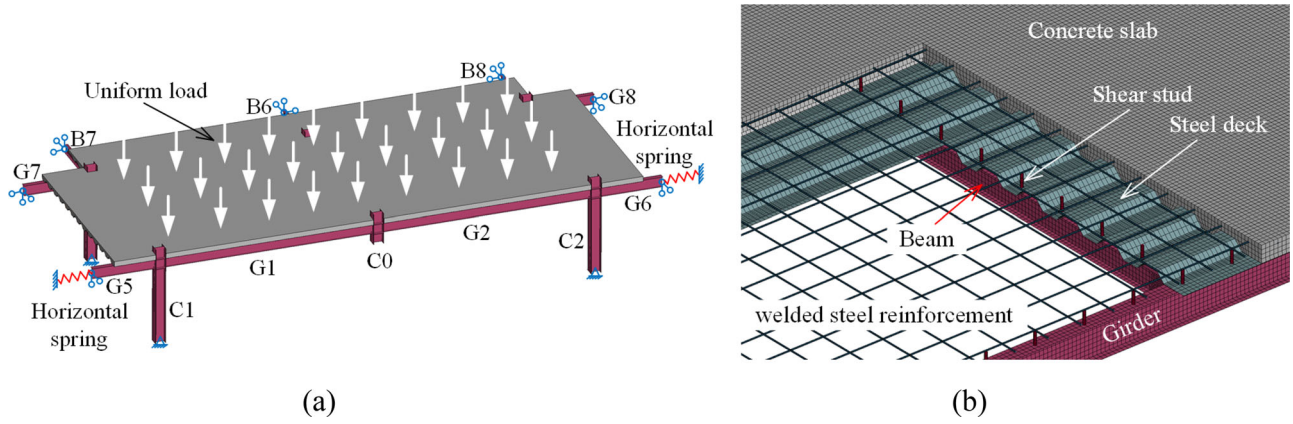

Figure 5. FEM details: (a) overall view of the model, (b) finite element mesh details.

Table 1. Mechanical properties of steel materials for different elements in various structural members.

Steel member	Location	Yield stress (MPa)	Ultimate stress (MPa)	Elongation (mm/mm)
Girder	Flange	390	536	0.31
	Web	419	557	0.31
Beam	Flange	365	517	0.31
	Web	400	535	0.32
Column	Flange	373	531	0.32
	Web	395	546	0.31
Rebar	Slab	596	672	0.07
Steel deck	Slab	320	380	0.38
Shear stud	Slab	320	400	0.14
Bolt	Connection	940	1040	0.10

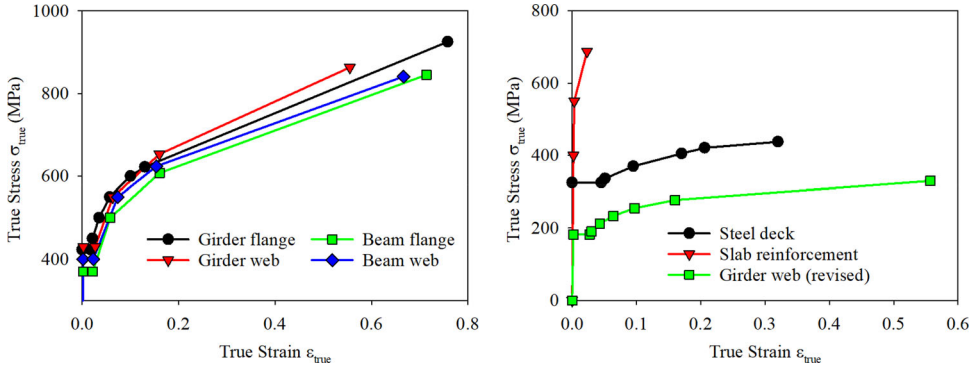

Figure 6. σ-ε curves of steel materials.

Based on the result in Figure 11, increasing the horizontal boundary constraint at the girder end would lead to premature failure at the girder-to-column connection. The development of the catenary action is related to the axial force in the girder, and the chord rotation angle of the girder. The deformation corresponding to girder-to-column connection failure limits catenary action and therefore limits the strength at collapse. If the failure displacement of the catenary action is identical to that of the membrane action, the vertical resistance would be the largest. However, if the girder end is not constrained, the tensile force in the girder is marginal compared with that in the other two cases. Even though the vertical resistance keeps increasing, the maximum resistance is not exceeded the other two cases. But, for the 'Not constrained' case, the large failure displacement of the girder-to-column connection is a specific advantage. As the progressive collapse is a dynamic process, the sudden drop of the load caused by the premature connection failure may exacerbate the dynamic response of the entire structure.

In the 'Completely constrained' case, the vertical resistance is mainly limited by the rotational capacity of the WFBW connection. In order to improve the rotational capacity of the connection, the WFBW connection is replaced by the reduced beam-section (RBS) connection (Figure 12(a)). In the experimental test conducted by Lew, Main, Robert, Sadek, and Chiarito (2012), the RBS connection exhibited a better rotational capacity and load-carrying capacity than the WFBW connection. However, different beam cross-sections were used for these two connections in the test. In this paper, the RBS connection is using the same girder cross-section with the WFBW connection. First of all, the behaviours of these connections are compared using a half-span connection model (Figure 12(b)). The beam-column-beam subassembly with two half-span beams is usually

used to investigate the connection performance under the progressive collapse scenario (Qin, Wang, Chen, & Bao, 2015). In this study, the column is relatively strong, and the deformation of the column at the connection can be neglected. For this reason, the beam-column-beam subassembly is reduced to a half-span connection model (Figure 12(b)). The vertical displacement-controlled load is applied at the girder end, while the horizontal displacement at the girder end is horizontally constrained.

Figure 12(c) illustrates the load-displacement curves and failure modes of these two connections. The failure of the WFBW connection has two stages: (i) bottom flange fracture (first peak), (ii) bolted web fracture and top flange fracture (second peak). For the RBS connection, the crack firstly occurs in the bottom flange at the RBS, then the crack abruptly propagates to the entire cross-section. Therefore, only one peak is achieved for the RBS connection. However, the corresponding displacement at the crack initiation point of RBS connection is approximately equal to 2.4 times that at the first peak of the WFBW connection and is similar to the displacement at the second peak of WFBW connection. The maximum resistance of the RBS connection is about 1.8 times the WFBW connection. The 'Completely constrained' case has been recomputed with the RBS connection. The mesh details of the RBS connection and the load-displacement curves of the floor systems with the WFBW connection or RBS connection are shown in Figure 13. After replacing the WFBW connection with RBS connection, the rotation capacity and load-carrying capacity of the floor system is improved by 19.2% and 17.0%, respectively. Therefore, if the beams connected to the removed column are completely constrained, the RBS connection can be used in these beams to improve the collapse resistance of the floor system. Apart from the RBS connection, other retrofitted connections with satisfactory rotational capacity and resistance (Ghorbanzadeh, Bregoli, Vasdravellis, & Karavasilis, 2019; Qin et al., 2015; Wei et al., 2019) can also be selected.

Based on the discussion above, following strategies can be used to improve the robustness of the composite floor system: (1) if the horizontal movements of the beams connected to the removed column are constrained by the neighbouring bays, retrofitted connections with adequate rotational capacity and load-carrying capacity are recommended to use in these beams to improve the catenary action; (2) if the horizontal movements of the beams connected to the removed column are not constrained, the section of these beams needs to be enlarged to improve the flexural resistance.

Table 2. Material properties of concrete.

Compressive strength (MPa)	Tensile strength (MPa)	Fracture energy (N/mm)	Elastic modulus (MPa)
26	2.7	0.131	29664
40	3.5	0.142	34129
60	4.6	0.153	39068

4.2.2. Boundary condition and continuity of steel deck

Steel deck thickness plays a vital role in the developing of the tensile membrane action (Sadek et al., 2008). As shown in Figure 14(a), in the common practice, two separate steel decks usually connect on the top flange of the beam by overlapping. While the shear stud is welded to the beam top flange, the two overlapped steel decks are melted and welded at the bottom of the shear stud. This overlapping butt joint is termed 'discontinuous'. In the experimental test mentioned before, the steel deck is continuous in the girder axis direction, which is named as the 'continuous' case. As depicted in Figure 14(b), the butt joint in the steel deck is simulated by reserving the deck elements connected to the shear studs on the beam top flange, and other deck elements intersected with the beam web plane are deleted. In Figure 14(b), the load-displacement response of these deck elements is determined by a butt joint simulation, in which, the initial distance between the centre of the shear stud and the deck edge is equal to twice the length of the shear stud diameter. In the floor test mentioned above, the steel deck is not constrained to the peripheral beams, so, the tensile membrane action could not be fully developed in this test. To investigate this behaviour, the horizontal movement at the steel deck is constrained in the floor model, which is named as 'constraint deck'. In order to investigate the boundary condition of the welded steel reinforcement in the test, a case 'constraint deck + bar' is also simulated, in

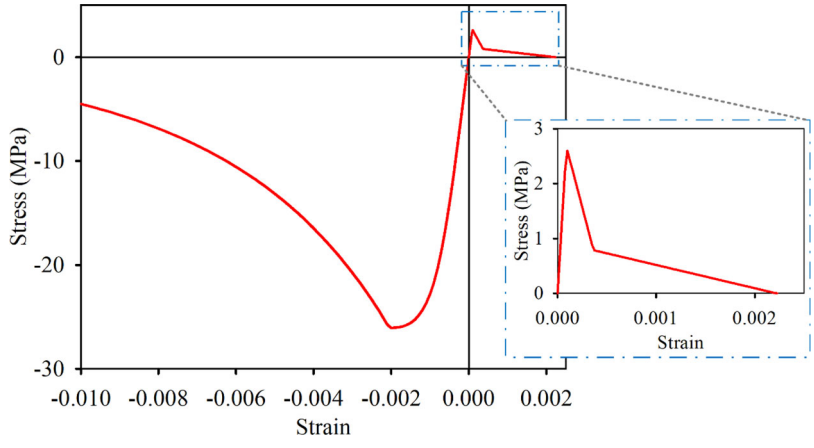

Figure 7. Stress-strain curve of concrete.

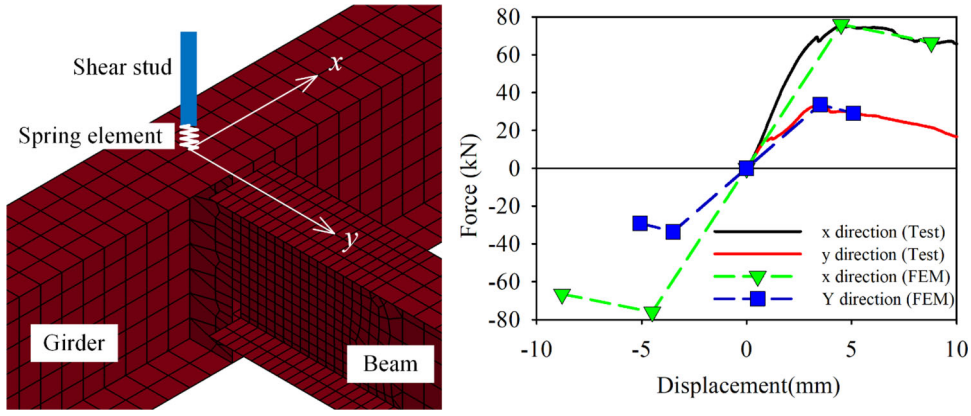

Figure 8. Shear responses of shear stud.

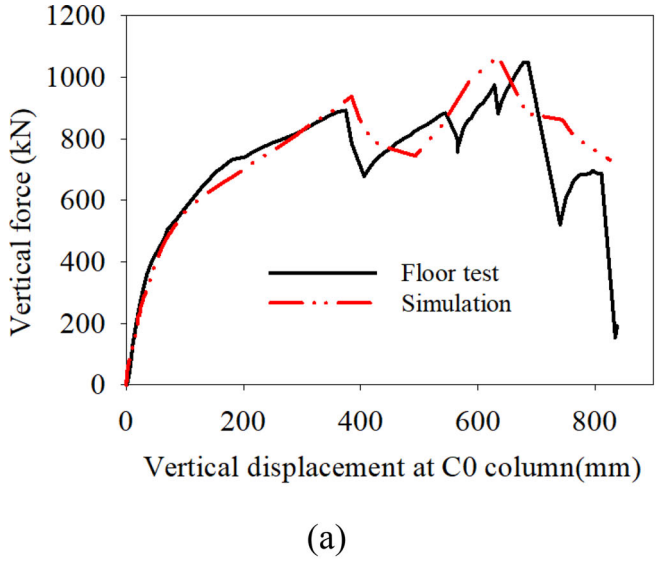

(a)

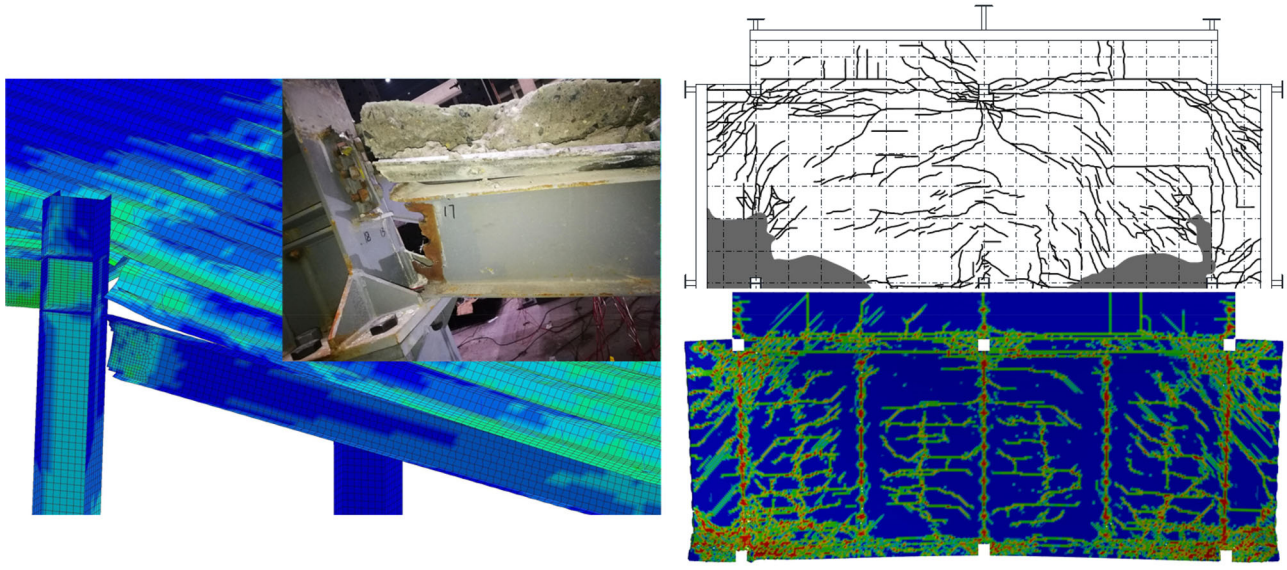

(b)

Figure 9. Comparison between FEM and experimental test: (a) load-displacement curve, (b) failure phenomenon in FEM.

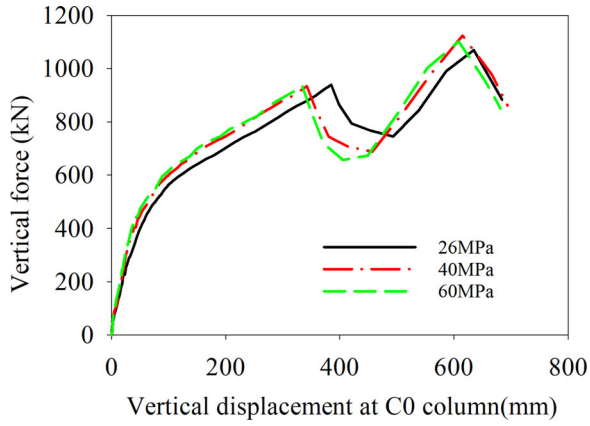

Figure 10. Influence of the concrete strength.

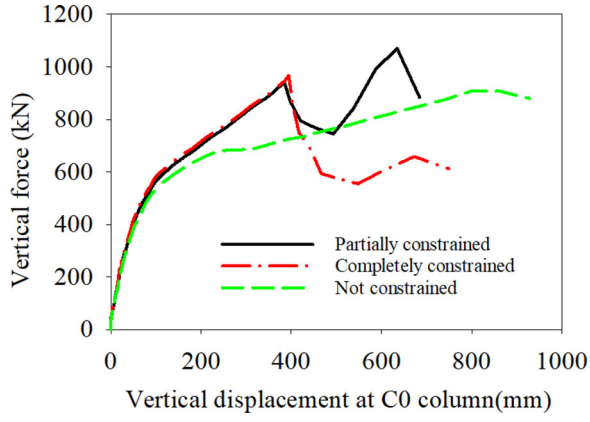

Figure 11. Influence of the horizontal constraint at the end of G5 and G6 girders.

Table 3. Comparison of the vertical resistance under different horizontal constraint conditions.

	Completely constrained	Partially constrained	Not constrained
Ultimate vertical force (kN)	946	1070	908
Vertical displacement (mm)	396	635	799

which, both the horizontal movement of the steel deck and welded steel reinforcement is constrained.

The comparison of these cases is illustrated in Figure 15. The floor capacity of the 'continuous' case is enhancing by 10.4% compared with the case with the butt joint, while the enhancement percentage of the 'constraint deck' and 'constraint deck + bar' cases are roughly equal to 40%. By comparing the 'constraint deck' and 'constraint deck + bar' cases, the lateral constraint of the welded steel reinforcement does not affect the floor capacity. Based on the results in Figure 15, it is noticeable increasing the boundary constraint and the continuity of the steel deck could significantly improve the vertical resistance of the composite floor at the large deformation stage, which is because the development of the tensile membrane force in the steel deck relied on these two factors. The importance of the continuity of the steel deck is also noted by Hadjioannou (2015). Compared with the evident effect of constraining the boundary of the steel deck, the increasing of the vertical resistance after constraining the rebar is negligible. This is because the rebar is mainly under compression, or the tensile strain in the rebar is relatively low; hence, rebar could not contribute to the development of the tensile membrane action. Therefore, the steel deck is the primary source of the tensile membrane action.

4.3. Influence of steel deck thickness

Generally, in China, the thickness of the trapezoidal steel deck used in the composite floor system is varied between 0.75 mm and 1.5 mm (CECS 273-2010, 2010). Therefore, the effect of the steel deck thickness is studied by comparing the composite floor substructures with the typical deck thickness of 0.9 mm, 1.2 mm, or 1.5 mm. The case with 1.2 mm thick deck is the baseline for comparison, which is identical to the experimental test.

Figure 16 presents the results of these three simulation cases. The vertical resistances of the 1.2 mm and 1.5 mm thick deck simulations are 8.7% and 14.6% higher than that of the 0.9 mm thick deck simulation, respectively. By constraining the horizontal movements of the steel deck, the vertical resistance of the floor system could be enhanced by 21.1%, 19.1% and 18.6% for the cases with 0.9 mm, 1.2 mm and 1.5 mm thick steel decks, respectively. After constraining the lateral movement of the steel deck, comparing with the 0.9 mm case, increasing the steel deck thickness to 1.2 mm and 1.5 mm could improve the floor capacity by 6.9% and 12.3%, respectively. Both increasing the continuity and the thickness of the steel deck could improve the floor capacity by generating more tensile membrane action.

As mentioned above, tensile membrane action is mainly provided by the steel deck, therefore, it was evident that increasing the thickness of the steel deck could enhance the vertical resistance at the large deformation stage, which is also been confirmed by Alashker et al. (2010). However, compared with the numerical results of Alashker et al. (2010), increasing the steel deck thickness has a limited effect on the flexural resistance at the early stage. This is because, in the current study, the flexural resistance at the early stage was mainly contributed by the rigid girder-to-column connection, while the flexural resistance provided by the pin connection used in the simulation of Alashker et al. (2010) is relatively minor.

4.4. Influence of slab reinforcement ratio and layouts

Floor systems with different diameters of the steel reinforcement are used to investigate the influence of slab reinforcement ratio, while other parameters such as the material property of the steel reinforcement, the spacing of the steel reinforcement are unchanged. The result from the case with 8 mm diameter steel reinforcement is used as the benchmark and is compared with the results from the 6 mm case and 10 mm case. As shown in Figure 17, compared with the 6 mm case, the vertical resistances at the large deformation stage are improved by 6.8% and 10.8% in the 8 mm case and 10 mm case, respectively. After constraining the lateral movement of the steel deck, the floor capacity of all cases is improved by 12.9%~21.1%. However, with the steel deck

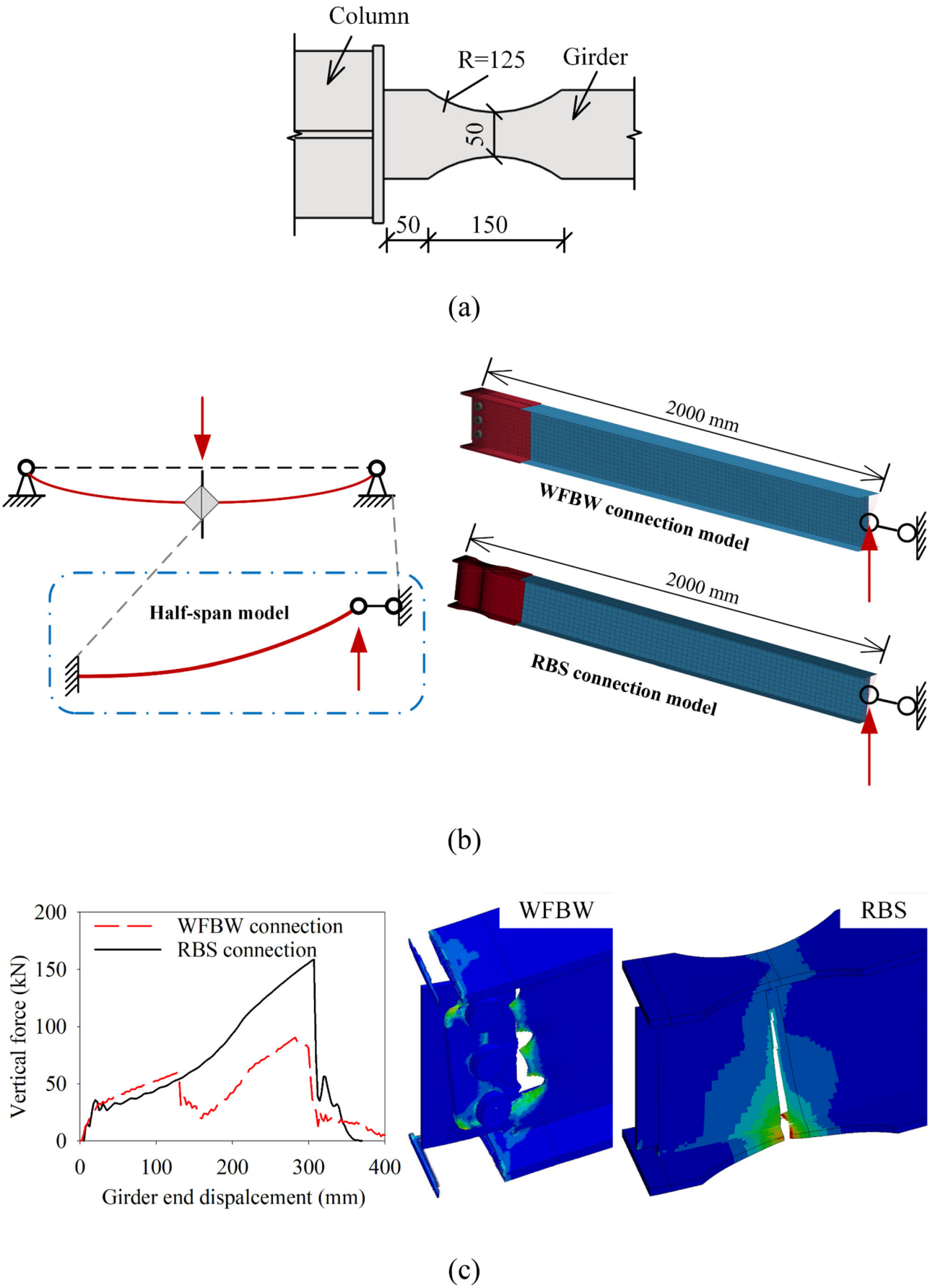

Figure 12. Comparison between the WFBW connection and RBS connection: (a) dimensions of RBS connection, (b) half-span connection model, (b) load-displacement curve.

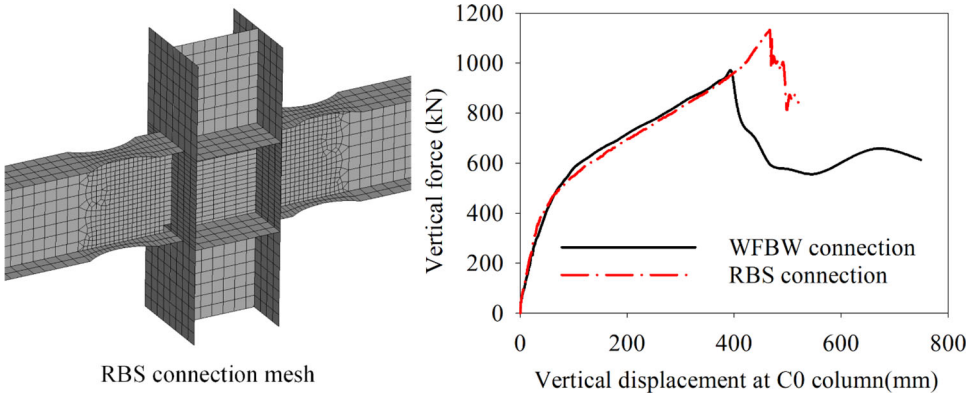

Figure 13. Comparison between floor systems with WFBW connection and RBS connection.

constrained, the floor capacity of the 8 mm and 10 mm cases is only about 3.4%~5.0% higher than that of the 6 mm case.

The effect of the layout of the steel reinforcement is studied by comparing three grid sizes of the steel reinforcement, i.e., 100 × 100 mm, 200 × 200 mm, 300 × 300 mm. The 200 × 200 mm grid size is selected as the baseline for comparison. In these three cases, the cross area of the steel reinforcement at per unit width slab keeps the same, which is 0.25 mm^2/mm. In other words, the slab reinforcement ratio is unchanged in these three cases. As shown in Figure 18, compared with the result from the case with 200 × 200 mm grid size, decreasing the grid size to 100 × 100 mm could increase the vertical resistance by 3.8%, and increasing the grid size to 300 × 300 mm could weaken the vertical resistance by 8.0%. However, after constraining the steel deck, the vertical resistances are almost identical for these three cases.

Based on the numerical results in this section, when the boundary of the steel deck is not constrained, increasing the rebar diameter and a relatively finer grid size of the slab rebar could improve the load-carrying capacity of the floor system in the large deformation stage. This improvement is more significant when increasing the rebar diameter from 6 mm to 8 mm and decreasing the rebar mesh from '300 × 300 mm' to '200 × 200 mm', but the mechanism behind these two situations is different. The improvement of the vertical resistance when increasing the rebar diameter from 6 mm to 8 mm is mainly contributed by enhanced tensile membrane force provided by the rebar. However, as mentioned above, the tensile strain in the rebar is not fully developed; therefore, increasing the rebar diameter from 8 mm to 10 mm has a limited effect on the vertical resistance. The improvement of the vertical resistance when decreasing the rebar mesh from the '300 × 300 mm' to '200 × 200 mm' is due to the punching failure of the slab has been prevented. In the '300 × 300 mm' case, the concrete elements inside the rebar grid are crushed caused by the shear failure at the final stage. However, this phenomenon is avoided in the '200 × 200 mm' case and '100 × 100 mm' case. Because the rebar ratio is identical in these three cases, the vertical resistance between '200 × 200 mm' case and '100 × 100 mm' case is similar.

According to JGJ 114-2014 (2014), the grid size of the welded steel reinforcement cannot exceed 200 mm while the slab thickness is less than 150 mm, and the grid size cannot exceed 300 mm if the slab thickness is more than 150 mm. Hence, if the composite slab is correctly designed, the shear failure of the slab can be avoided, and altering the grid size of the welded steel reinforcement would have limited influence on the collapse resistance. When the boundary of the steel deck is constrained, both increasing the rebar diameter and decreasing the rebar mesh could not improve the load-carrying capacity of the floor system in the large deformation stage. This was because the tensile membrane force provided by the rebar is negligible compared with that provided by the steel deck, and the shear failure of the slab is also prevented by the constrained steel deck.

4.5. Influence of shear stud spacing

Shear stud is crucially essential to connect the floor slab with the steel beam, and then these two parts can work collaboratively through the composite action formed by the shear stud connection. In the experimental test, the shear stud spacing parallel to the girder axis is 300 mm, and the shear stud spacing on the beam is 305 mm, one per rib. The simulation case identical to the test is named as '300 mm'. The case with doubled shear stud numbers is named as '150 mm', which shear stud spacing on the girder is 150 mm, and each deck rib on the beam has two shear studs.

As shown in Figure 19, the vertical resistance of the '150 mm' case is 7.1% higher than the '300 mm' case. At the same time, the fracture displacement of the top flange at the G1-C1 connection is decreased to 86.7% of the '300 mm' case. When the lateral movement of the steel deck is constrained, the vertical resistance of the floor system in each case is improved by about 12%. With the steel deck horizontally constrained, a finer shear stud arrangement (150 mm case) could also improve the floor resistance by 7.9% when compared with the 300 mm case.

The increased flexural rigidity before the girder flange fracture is attributed to the enhanced flexural resistance after increasing the number of the shear stud. After the girder flange fracture, the vertical resistance is mainly dependent on the catenary action and tensile membrane action. The development of the catenary action relies on the tensile force in the girder, which comes from two sources: (1) the tensile force developed by the residual section at the girder-to-column connection; (2) the tensile force transferred from

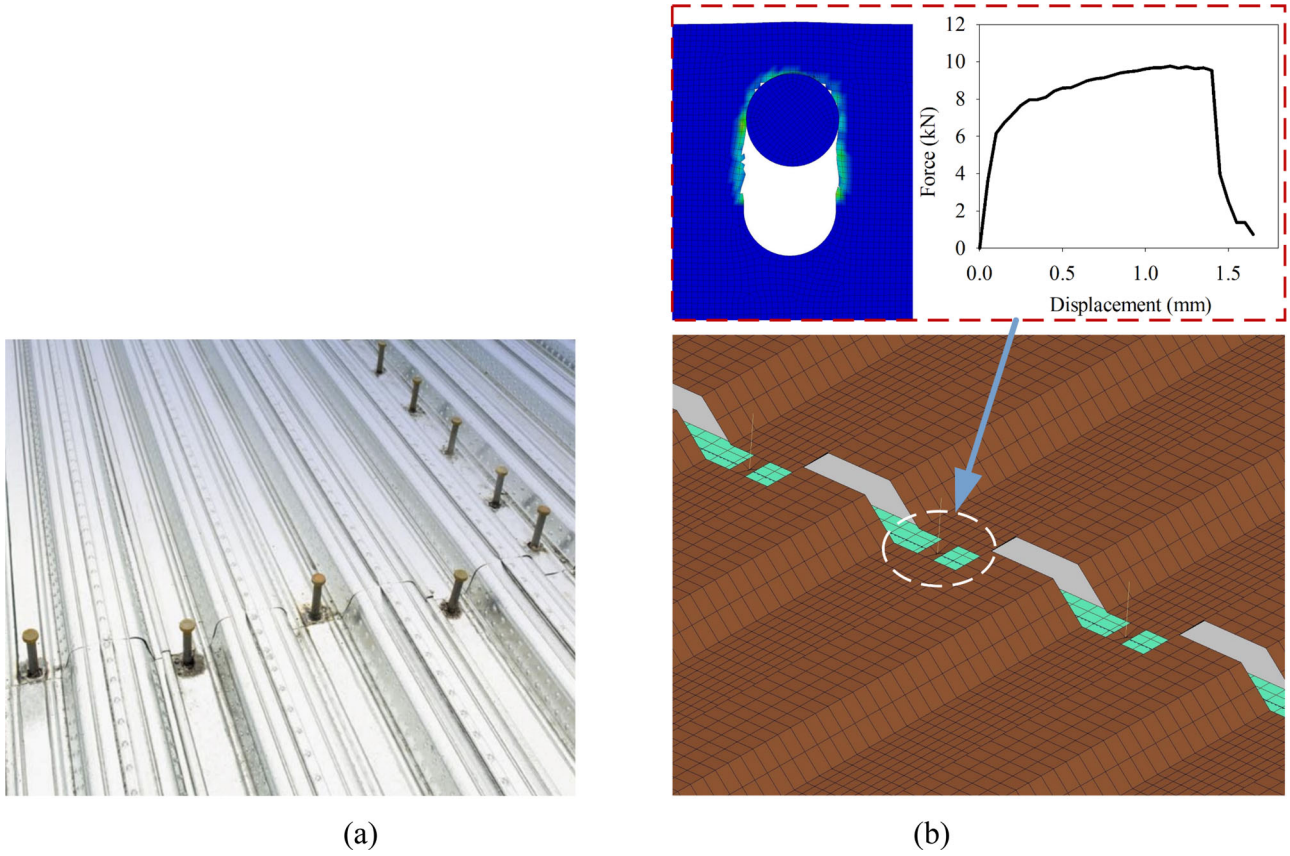

Figure 14. Modeling of the discontinuous steel deck: (a) butt joint in steel deck; (b) modeling details of the butt joint.

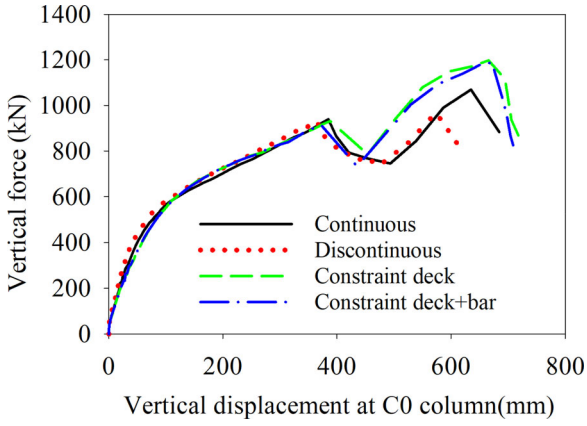

Figure 15. Influence of the steel deck continuity.

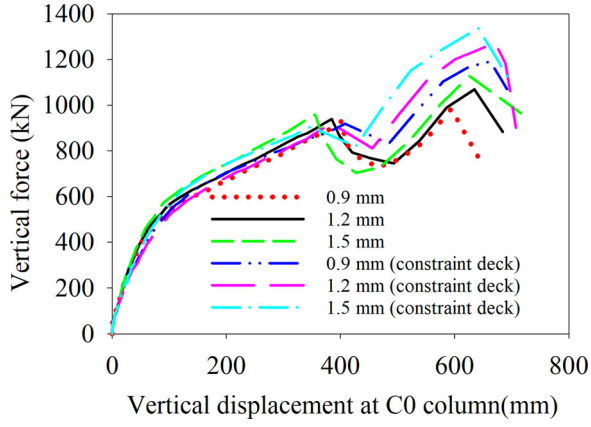

Figure 16. Influence of the steel deck thickness.

the composite slab. The tensile force transferred from the composite slab is increased after decreasing the spacing of the shear stud, and the catenary action has also been improved simultaneously. Hence, the improvement of the vertical resistance after decreasing the spacing of the shear stud is owing to the enhanced catenary action.

4.6. Measures to improve progressive collapse resistance

Based on the above parametric studies, it can be concluded that the ways to increase the progressive collapse resistance of the composite floor system are increasing the continuity of the steel deck, increasing the steel deck thickness, increasing the number of the shear stud, increasing the rebar diameter, and decreasing the grid size of the welded steel reinforcement. Increasing the concrete strength has a limited effect on the resistance capacity of the composite floor system under the middle edge column scenario; however, it may improve the dynamic response of the structure subjected to the sudden column loss.

Considering the steel quantities used in the composite floor system, increasing the continuity of the steel deck and decreasing the grid size of the welded steel reinforcement are the best choices, as the steel quantities are not increased. Whereas, as mentioned above, altering the grid size of the

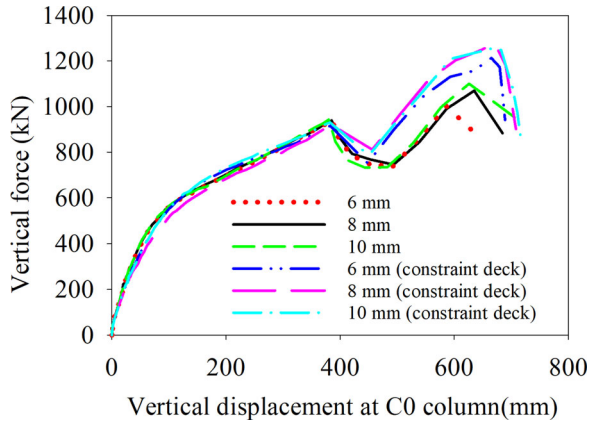

Figure 17. Influence of the steel reinforcement diameter.

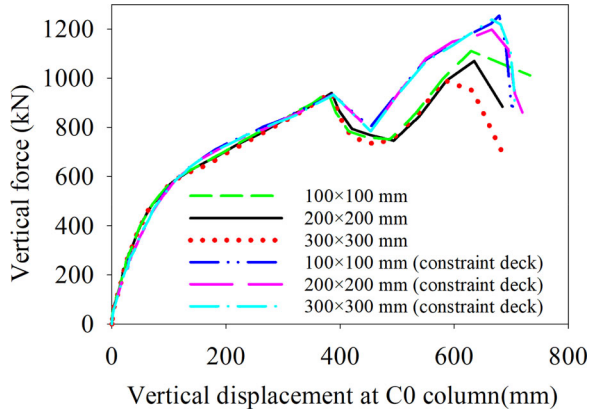

Figure 18. Influence of the steel reinforcement layout.

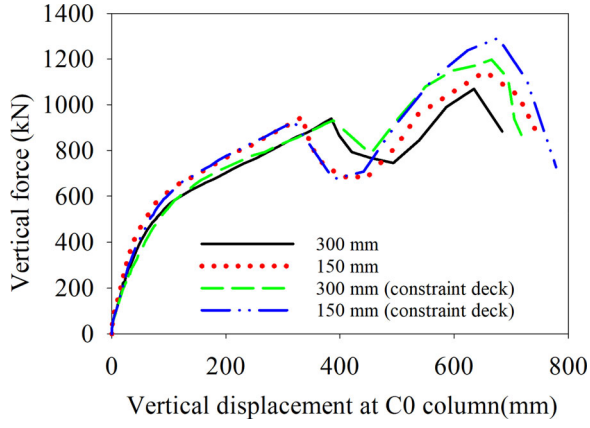

Figure 19. Influence of the shear stud spacing.

welded steel reinforcement has limited influence on the collapse resistance when the composite slab is properly designed. Therefore, increasing the continuity of the steel deck is the only remaining best option. Unfortunately, the significance of the continuity of the steel deck has not been attracted much attention. Generally, the steel deck is simplified connected through the shear stud (Figure 12(a)), which is a huge waste of the progressive collapse resistance. It is recommended that the steel decks need to be completely welded with each other in the overlap area. Moreover, the steel decks also need to be completely welded to the peripheral beams at the boundary region of the slab.

5. Conclusions

In this paper, high fidelity numerical models are used to study the progressive collapse resistance of one-story steel-concrete composite floor system with the rigid girder-to-column connection under middle edge column removal scenarios. The numerical models are validated through comparisons with test data and employed to investigate the parameters affecting the progressive collapse resistance of the steel-concrete composite floor system. The investigated parameters include the lateral restraint stiffness at the horizontal boundaries, concrete strength, slab reinforcement ratio, slab reinforcement layout, steel deck thickness, the continuity of the steel deck, and the shear stud spacing.

The main conclusions drawn from the numerical investigation are as follows:

- Increasing concrete strength can slightly improve the initial stiffness at the flexural stage, but cannot affect the development of the catenary action and tensile membrane action.
- Increasing the stiffness of the horizontal boundary constraint at the girder ends may not useful for improving the vertical resistance of the composite floor system. If the girder ends are constrained, sufficient rotational capacity of the girder-to-column connection is crucial for the developing of the catenary action.
- Improving the continuity of the steel deck, constraining the steel deck's horizontal boundary movement, and increasing the steel deck thickness can significantly enhance the progressive collapse resistance of the composite floor system.
- Increasing the rebar ratio is useful for improving the tensile membrane action when the steel deck is not horizontally constrained.
- If the composite slab is correctly designed according to the code, the shear failure of the slab can be avoided, and altering the grid size of the welded steel reinforcement would have limited influence on the floor resistance.
- Increasing the number of the shear stud can improve the floor resistance by enhancing the catenary action at the large deformation stage.

Acknowledgements

Any opinions, findings, conclusions, and recommendations expressed in this paper are those of the authors and do not necessarily reflect the views of the sponsors.

Disclosure statement

No potential conflict of interest was reported by the authors.

Funding

The research presented in this paper was sponsored by the State Key Laboratory of Disaster Reduction in Civil Engineering (Tongji University) through Grant Nos. SLDRCE19-A-03 and Natural Science Foundation of China (NSFC) through Grant No. 51378380.

References

Alashker, Y., & El-Tawil, S. (2011). A design-oriented model for the collapse resistance of composite floors subjected to column loss. *Journal of Constructional Steel Research*, *67*(1), 84–92. doi:10.1016/j.jcsr.2010.07.008

Alashker, Y., El-Tawil, S., & Sadek, F. (2010). Progressive collapse resistance of steel-concrete composite floors. *Journal of Structural Engineering*, *136*(10), 1187–1196. doi:10.1061/(ASCE)ST.1943-541X.0000230

Bao, Y., Main, J. A., & Noh, S. Y. (2017). Evaluation of structural robustness against column loss: Methodology and application to RC frame buildings. *Journal of Structural Engineering*, *143*(8), 04017066. doi:10.1061/(ASCE)ST.1943-541X.0001795

Belytschko, T., Lin, J. I., & Chen-Shyh, T. (1984). Explicit algorithms for the nonlinear dynamics of shells. *Computer Methods in Applied Mechanics and Engineering*, *42*(2), 225–251. doi:10.1016/0045-7825(84)90026-4

Botte, W., Gouverneur, D., Caspeele, R., & Taerwe, L. (2015). Influence of design parameters on tensile membrane action in reinforced concrete slabs. *Structural Engineering International*, *25*(1), 50–60. doi:10.2749/101686614X14043795570174

CEB-FIP. (2010). *CEB-FIP model code 2010, design code*. Telford: Author.

CECS 273-2010. (2010). *Code for composite slabs design and construction*. Beijing: Branch of the Association of Metallurgy of the People's Republic of China.

Eurocode, C. E. N. (2004). *Eurocode 4: Design of composite steel and concrete structures – Part 1–1: General rules and rules for buildings*. London, UK: British Standards Institution.

Fu, F. (2010). 3-D nonlinear dynamic progressive collapse analysis of multi-storey steel composite frame buildings - Parametric study. *Engineering Structures*, *32*(12), 3974–3980. doi:10.1016/j.engstruct.2010.09.008

Fu, Q. N., Tan, K. H., Zhou, X. H., & Yang, B. (2017). Load-resisting mechanisms of 3D composite floor systems under internal column-removal scenario. *Engineering Structures*, *148*, 357–372.

Fu, Q. N., Tan, K. H., Zhou, X. H., & Yang, B. (2018). Three-dimensional composite floor systems under column-removal scenarios. *Journal of Structural Engineering*, *144*(10), 04018196. doi:10.1061/(ASCE)ST.1943-541X.0002197

Gerasimidis, S. (2014). Analytical assessment of steel frames progressive collapse vulnerability to corner column loss. *Journal of Constructional Steel Research*, *95*, 1–9. doi:10.1016/j.jcsr.2013.11.012

Gerasimidis, S., Deodatis, G., Kontoroupi, T., & Ettouney, M. (2015). Loss-of-stability induced progressive collapse modes in 3D steel moment frames. *Structure and Infrastructure Engineering*, *11*(3), 334–344. doi:10.1080/15732479.2014.885063

Gerasimidis, S., Deodatis, G., Yan, Y., & Ettouney, M. (2017). Global instability induced failure of tall steel moment frame buildings. *Journal of Performance of Constructed Facilities*, *31*(2), 04016082. doi:10.1061/(ASCE)CF.1943-5509.0000940

Ghorbanzadeh, B., Bregoli, G., Vasdravellis, G., & Karavasilis, T. L. (2019). Pilot experimental and numerical studies on a novel retrofit scheme for steel joints against progressive collapse. *Engineering Structures*, *200*, 109667. doi:10.1016/j.engstruct.2019.109667

Gouverneur, D., Caspeele, R., & Taerwe, L. (2013a). Experimental investigation of the load–displacement behaviour under catenary action in a restrained reinforced concrete slab strip. *Engineering Structures*, *49*, 1007–1016. doi:10.1016/j.engstruct.2012.12.045

Gouverneur, D., Caspeele, R., & Taerwe, L. (2013b). Effect of reinforcement curtailment on deflections, strain and crack development in RC slabs under catenary action. *Magazine of Concrete Research*, *65*(22), 1336–1347. doi:10.1680/macr.13.00141

Gouverneur, D., Caspeele, R., & Taerwe, L. (2015). Strain and crack development in continuous reinforced concrete slabs subjected to catenary action. *Structural Engineering and Mechanics*, *53*(1), 173–188. doi:10.12989/sem.2015.53.1.173

Grassl, P., & Jirásek, M. (2006). Damage-plastic model for concrete failure. *International Journal of Solids and Structures*, *43*(22-23), 7166–7196. doi:10.1016/j.ijsolstr.2006.06.032

Grassl, P., Xenos, D., Nyström, U., Rempling, R., & Gylltoft, K. (2013). CDPM2: A damage-plasticity approach to modelling the failure of concrete. *International Journal of Solids and Structures*, *50*(24), 3805–3816. doi:10.1016/j.ijsolstr.2013.07.008

Hadjioannou, M., Donahue, S., Williamson, E. B., & Engelhardt, M. D. (2018). Large-scale experimental tests of composite steel floor systems subjected to column loss scenarios. *Journal of Structural Engineering*, *144*(2), 04017184. doi:10.1061/(ASCE)ST.1943-541X.0001929

Hadjioannou, M. (2015). Large-scale testing and numerical simulations of composite floor slabs under progressive collapse scenarios (Doctoral dissertation). University of Texas at Austin, Austin, TX.

Hallquist, J. O. (2016). *LS-DYNA keyword user's manual (Version R9.1)*. Livermore, CA: Livermore Software Technology Corporation.

Hayes, B. (1968). Allowing for membrane action in the plastic analysis of rectangular reinforced concrete slabs. *Magazine of Concrete Research*, *20*(65), 205–212. doi:10.1680/macr.1968.20.65.205

Hughes, T. J., & Liu, W. K. (1981a). Nonlinear finite element analysis of shells: Part I. Three-dimensional shells. *Computer Methods in Applied Mechanics and Engineering*, *26*(3), 331–362. doi:10.1016/0045-7825(81)90121-3

Hughes, T. J., & Liu, W. K. (1981b). Nonlinear finite element analysis of shells-part II. two-dimensional shells. *Computer Methods in Applied Mechanics and Engineering*, *27*(2), 167–181. doi:10.1016/0045-7825(81)90148-1

JGJ 114-2014. (2014). *Technical specification for concrete structures reinforced with welded steel fabric*. Beijing: Ministry of Housing and Urban-Rural Development of the People's Republic of China.

Johnson, E. S., Meissner, J. E., & Fahnestock, L. A. (2016). Experimental behavior of a half-scale steel concrete composite floor system subjected to column removal scenarios. *Journal of Structural Engineering*, *142*(2), 04015133. doi:10.1061/(ASCE)ST.1943-541X.0001398

Krieg, R. D., & Key, S. W. (1976). Implementation of a time independent plasticity theory into structural computer programs. *Constitutive equations in viscoplasticity: Computational and Engineering Aspects*. *20*, 125–137.

Lew, H. S., Main, J. A., Robert, S. D., Sadek, F., & Chiarito, V. P. (2012). Performance of Steel Moment Connections under a Column Removal Scenario. I: Experiments. *Journal of Structural Engineering*, *139*(1), 98–107. doi:10.1061/(ASCE)ST.1943-541X.0000618.

Mitchell, D., & Cook, W. D. (1984). Preventing progressive collapse of slab structures. *Journal of Structural Engineering*, *110*(7), 1513–1532. doi:10.1061/(ASCE)0733-9445(1984)110:7(1513)

Park, R. (1964a). Tensile membrane behaviour of uniformly loaded rectangular reinforced concrete slabs with fully restrained edges. *Magazine of Concrete Research*, *16*(46), 39–44. doi:10.1680/macr.1964.16.46.39

Park, R. (1964b). Ultimate strength of rectangular concrete slabs under short-term uniform loading with edges restrained against lateral movement. *Proceedings of the Institution of Civil Engineers*, *28*(2), 125–150. doi:10.1680/iicep.1964.10109

Park, R. (1965). The lateral stiffness and strength required to ensure membrane action at the ultimate load of a reinforced concrete slab-and-beam floor. *Magazine of Concrete Research*, *17*(50), 29–38. doi:10.1680/macr.1965.17.50.29

Qian, K., Li, B., & Ma, J. X. (2015). Load-carrying mechanism to resist progressive collapse of RC buildings. *Journal of Structural Engineering*, *141*(2), 04014107. doi:10.1061/(ASCE)ST.1943-541X.0001046

Qin, X., Wang, W., Chen, Y., & Bao, Y. (2015). Experimental study of through diaphragm connection types under a column removal scenario. *Journal of Constructional Steel Research*, *112*, 293–304. doi:10.1016/j.jcsr.2015.05.022

Sadek, F., El-Tawil, S., & Lew, H. S. (2008). Robustness of composite floor systems with shear connections: Modeling, simulation, and evaluation. *Journal of Structural Engineering*, *134*(11), 1717–1725. doi:10.1061/(ASCE)0733-9445(2008)134:11(1717)

Sawczuk, A., & Winnicki, L. (1965). Plastic behavior of simply supported reinforced concrete plates at moderately large deflections. *International Journal of Solids and Structures*, *1*(1), 97–111. doi:10.1016/0020-7683(65)90019-3

Tahmasebinia, F., Ranzi, G., & Zona, A. (2011). A probabilistic three-dimensional finite element study on simply-supported composite floor beams. *Australian Journal of Structural Engineering*, *12*(3), 251–262. doi:10.7158/S11-107.2012.12.3

Wang, J., Wang, W., & Bao, Y. (2020). Full-scale test of a steel-concrete composite floor system with moment-resisting connections under a middle edge column removal scenario. *Journal of Structural Engineering*, doi: 10.1061/(ASCE)ST.1943-541X.0002630. (Accepted).

Wang, J., Wang, W., Bao, Y., & Lehman, D. (2019). Full-scale test of a steel moment-resisting frame with composite floor under a penultimate edge column removal scenario. *Journal of Constructional Steel Research*, *162*, 105717. doi:10.1016/j.jcsr.2019.105717

Wang, J., Wang, W., & Qian, X. (2019). Progressive collapse simulation of the steel-concrete composite floor system considering ductile fracture of steel. *Engineering Structures*, *200*, 109701. doi:10.1016/j.engstruct.2019.109701

Wei, J. P., Tian, L. M., Hao, J. P., Li, W., Zhang, C. B., & Li, T. J. (2019). Novel principle for improving performance of steel frame structures in column-loss scenario. *Journal of Constructional Steel Research*, *163*, 105768. doi:10.1016/j.jcsr.2019.105768

Yi, W. J., Zhang, F. Z., & Kunnath, S. K. (2014). Progressive collapse performance of RC flat plate frame structures. *Journal of Structural Engineering*, *140*(9), 04014048. doi:10.1061/(ASCE)ST.1943-541X.0000963